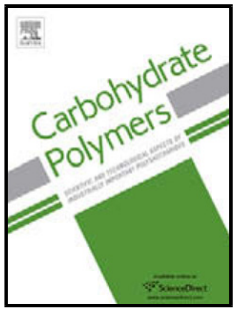

Title: Synthesis and antimicrobial properties of Zn-mineralized alginate nanocomposites

Authors: Ivana Malagurski, Steva Levic, Milena Pantic, Danka Matijasevic, Miodrag Mitric, Vladimir Pavlovic, Suzana Dimitrijevic-Brankovic

PII: S0144-8617(17)30194-7
DOI: http://dx.doi.org/doi:10.1016/j.carbpol.2017.02.064
Reference: CARP 12043

To appear in:

Received date: 21-11-2016
Revised date: 25-1-2017
Accepted date: 16-2-2017

Please cite this article as: Malagurski, Ivana., Levic, Steva., Pantic, Milena., Matijasevic, Danka., Mitric, Miodrag., Pavlovic, Vladimir., & Dimitrijevic-Brankovic, Suzana., Synthesis and antimicrobial properties of Zn-mineralized alginate nanocomposites.*Carbohydrate Polymers* http://dx.doi.org/10.1016/j.carbpol.2017.02.064

Synthesis and antimicrobial properties of Zn-mineralized alginate nanocomposites

Ivana Malagurski[a,*], Steva Levic[b], Milena Pantic[b], Danka Matijasevic[b], Miodrag Mitric[c], Vladimir Pavlovic[b], Suzana Dimitrijevic-Brankovic[a]

[a]*Faculty of Technology and Metallurgy, University of Belgrade, Karnegijeva 4, 11000 Belgrade, Serbia*

[b]*Faculty of Agriculture, University of Belgrade, Nemanjina 6, 11000 Belgrade, Serbia*

[c]*Vinca Institute of Nuclear Science, University of Belgrade, P.O. Box 522, 11001 Belgrade, Serbia*

Corresponding author: Ivana Malagurski

Tel: +381(0)11 3303788

Fax: +381(0)11 3370387

E-mail: madzovska@tmf.bg.ac.rs

Highlights

- Zn-mineralized alginate nanocomposites were produced in one-step method
- Presence of Zn-mineral phase has increased total nanocomposite Zn(II) content
- Stability and Zn(II) release are modulated by the presence of mineral phase
- Nanocomposites release Zn(II) inducing strong antimicrobial effect

Abstract

New bioactive and antimicrobial biomaterials were produced by alginate-mediated biomineralization with Zn-mineral phase. The synthesis procedure is simple, cost-effective and resulted in two different Zn-mineralized alginate nanocomposites, Zn-carbonate/Zn-alginate and Zn-phosphate/Zn-alginate. The presence of Zn-mineral phase and its type, have significantly affected nanocomposite morphology, stability, total metallic loading and potential to release Zn(II) in physiological environment. Antimicrobial experiments showed that both types of Zn-mineralized nanocomposites exhibit strong antimicrobial effect against *Escherichia coli*, *Staphylococcus aureus* and C*andida albicans.* These results suggest that alginate biomineralization, where minerals are salts of essential metallic ions like Zn(II), represents a good strategy for designing multifunctional biomaterials for potential biomedical applications.

Keywords: zinc, alginate, nanocomposite, biomineralization, antimicrobial activity

1. Introduction

Hydrogel-mediated biomineralization, as a nature-inspired design principle, represents a good platform for production and development of new, composite biomaterials (Asenath-Smith, Li, Keene, Seh, & Estroff, 2012). Mineralized biomaterials were studied either as model systems for biomineralization processes (*e.g.* model system of tooth formation (Busch, Schwarz, & Kniep, 2001), or scaffolds for bone tissue engineering (Xie et al., 2010). Ideally, a biopolymer for biomineralization studies should be biocompatible, structurally similar to an extracellular matrix and relatively abundant. A suitable candidate that meets aforementioned criteria is alginate.

Alginates represent a family of polysaccharides synthesized by brown algae and bacteria. They are linear copolymers of 1-4 linked β-D-mannuronic acid (M) and α-L-guluronic (G) units, organized into homopolymeric (M- and G-blocks) and heteropolymeric (MG-blocks) regions. The most important alginate characteristic, from biomedical perspective, is the ability to selectively bind divalent metal ions and form biocompatible and hydrophilic hydrogels (Donati & Paoletti, 2009) with wide biomedical applications (Tuan, Boland, & Tuli, 2003, Bouhadir, Alsberg, & Mooney, 2001; Qin, 2008). According to literature, several mineralized alginate-based biomaterials were successfully developed. It has been shown that mineralization of alginate in the presence of calcium and phosphate mineral precursors resulted in the formation of low crystalline hydroxyapatite, suitable for bone tissue engineering (Xie et al., 2010). Also, mineralized alginates were studied as cell and drugs delivery systems (Green et al., 2005; Shi, Zhang, Qi, & Cao, 2012).

By impregnating alginate hydrogel with stiffer phase like minerals one could make a composite with better mechanical properties and prolonged stability. Additionally, if these minerals are salts of essential metals like Zn, they could contribute to the functionality of the obtained composite.
Zinc is an essential trace element involved in growth, immune system functioning, neural development and antioxidative activity (Kaur, Gupta, Saraf, & Saraf, 2014). From the biomedical perspective, the most interesting are Zn roles in wound healing (Lansdown, Mirastschijski, Stubbs, Scanlon, & Ågren, 2007) and bone formation (Yamaguchi, 1998). Zn also exhibits strong antimicrobial activity against both Gram negative and Gram positive bacteria (Lemire, Harrison, & Turner, 2013). When present at superphysiological concentrations, zinc becomes a potent biocidal agent, which makes it an attractive antimicrobial component of biomaterials (Kasemets,

Ivas, Dubourguier, & Kahru, 2009). Mechanism of Zn(II) antimicrobial action are based on inhibition of conserved metabolic pathways involved in synthesis of essential biomolecules (*e.g.* site-specific inactivation of enzymes through destruction of Fe-S cluster) or antioxidant depletion by disulphide formation (Lemire et al., 2013).

So far, Zn has been used as bioactive and/or antimicrobial component of many biomaterials aimed for bone tissue engineering (Qiao et al., 2014; Salih, Patel, & Knowles, 2007) and wound dressings (Qin, 2008, Straccia, D'Ayala, Romano, & Laurienzo, 2015). However, the potential for therapeutic application of metal-based biomaterials is always limited due to potential toxicity or disturbance of other divalent metallic ions homeostasis (Willis et al., 2005).

The aim of this study was to test the hypothesis whether alginate-based biomineralization, with essential metal salts, Zn-minerals, can be considered a good platform for designing multifunctional nanocomposite biomaterials with tunable properties. In specific, we wanted to show that the presence of mineral phase within hydrogel influenced both: 1) nanocomposites properties (*in vitro* and thermal stability, total Zn(II) content and Zn(II) release kinetics); and 2) functionality (antimicrobial activity against *Escherichia coli*, *Staphylococcus aureus* and *Candida albicans).*

2. Materials and methods

2.1. Materials

Sodium chloride, disodium carbonate, disodium hydrogen phosphate dihydrate, zinc nitrate hexahydrate and Dulbecco's Modified Eagle Medium (DMEM) were obtained from Sigma Aldrich. Sodium alginate used in this study was low viscosity (A2158, M/G ratio of 1.56, degree of polymerization of 60-400, Sigma Aldrich). Nutrient Broth and Agar (NB and NA), Malt Extract Broth and Agar (MEB and MEA) were purchased from HiMedia Laboratories.

2.2. Synthesis of nanocomposite materials

Zn–mineralized alginate composite microbeads were prepared by procedure already described by Xie et al. (2010), with modifications. In brief, Na-alginate solution containing mineral precursors (1.9 % w/v Na-alginate, 100 mM Na_2HPO_4 or 100 mM Na_2CO_3) was extruded at a constant flow rate (40 ml/h) through a positively charged needle (20 G) into stirred, grounded gelling solution (100 mM $Zn(NO_3)_2$). The process was performed in an electric field generated between the

gelling solution and the needle, where electrostatic force breaks the polymer solution into small and uniform beads. The applied voltage was 6.5 kV. The gelation lasted for 24 h to provide optimal cross-linking and mineral phase formation. Non-mineralized Zn-alginate microbeads were produced according to the same procedure, using 1.9 % w/v Na-alginate solution as extrusion solution. Before further analysis, all types of microbeads were well rinsed in distilled water and saline solution (0.9 % NaCl) in order to remove loosely bound, non-structural Zn(II). Zn-mineral precipitates were made by mixing saturated solution of either Na_2CO_3 or Na_2HPO_4 with gelling solution (100 mM $Zn(NO_3)_2$). The precipitated minerals were thoroughly washed with deionized water, filtered and dried at room temperature. A summary of sample formulations and corresponding abbreviations are presented in **Table 1.**

2.3. Characterization

2.3.1. Optical microscopy

A binocular microscope Leica XTL-3 400D (Leica) equipped with a digital camera (DC 300, Leica) and image analysis program (IM 1000, Leica) was used to examine overall size and morphology of the obtained microbeads.

2.3.2. Scanning electron microscopy (SEM)

Microbeads surface and presence and morphology of mineral precipitates was examined using SEM. Prior examination, the microbeads were dried at room temperature. SEM of the whole, dried and gold coated microbeads was performed using a JEOL JSM-6390LV SEM (JEOL USA Inc.).

2.3.3. Fourier transform infrared spectroscopy (FTIR)

The FTIR spectra were recorded using a FTIR spectrometer IRAffinity-1 (SHIMADZU) at room temperature. Spectra were collected using KBr pellets in the spectral range 4.000-500 cm^{-1}, with the resolution of 4 cm^{-1}.

2.3.4. X-ray diffraction (XRD)

XRD data were collected on a Philips PW 1050 diffractometer with Cu-K$\alpha_{1,2}$ radiation (Ni filter) at room temperature. Measurements were done in 2θ range of 10-100° with scanning step width of 0.05° and 4 s/step.

2.3.5. Raman spectroscopy

Raman spectra were collected with a XploRA Raman spectrometer from Horiba Jobin Yvon. The system employed laser at 532 nm (maximum output power 20-25 mW). All measurements were realized using the 50x long working distance objective and spectrometer equipped with a 2400 gr/mm grating.

2.3.6. Thermogravimetric analysis (TGA)

Thermal stability was investigated using a SETARAM SETSYS Evolution 1750 instrument. The measurements were conducted at a heating rate of 20 C/min in a dynamic air atmosphere (flow rate 20 cm^3/min) and temperature range of 30-1000°C.

2.3.7. Total Zn(II) content in the microbeads

Total Zn(II) content of the non-mineralized and mineralized microbeads was determined using inductively coupled plasma optical emission spectroscopy (ICP-OES). 1 g of microbeads was incubated overnight in 9 ml of concentrated nitric acid (65 %). Proper dilutions of the acidic solutions were then measured by ICP-OES (Thermo).

2.4. Release kinetics

The capacity of different types of microbeads to release Zn(II) was investigated in physiological-like environment, 0.25 g of wet microbeads was placed into a flask with 5 ml of DMEM and then incubated at 37^{o}C under static conditions for 14 days. At different time points (incubation days 1, 3, 5, 7, 10 and 14), 4 ml of the incubation medium was removed and replaced with fresh medium. Concentration of the released Zn(II) was determined using ICP-OES.

2.5. Antimicrobial activity

The antimicrobial activity was tested against *Escherichia coli* ATCC 25922, *Staphylococcus aureus* ATCC 25923 and C*andida albicans* ATCC 10231. The cultivation/assay medium for *E. coli* and *S. aureus* was NB or NA, while for *C. albicans* MEB or MBA was used. The overnight

cultures, incubated at 30ºC for yeast and at 37ºC for bacterial strains, were used to achieve the initial concentration of approximately 10^5 CFU/ml.

Kinetics of inactivation was determined by Broth macrodilution method, according to Klančnik et al. (2010), with slight modifications. ZnAMB, ZnCMB and ZnPMB were added to microbial culture to reach final concentration of 300 mg/ml. The growth of tested microorganisms was followed by taking samples at 0, 1, 4, and 24 h and plating on NA/MEA after serial sample dilutions. The antimicrobial activity of ZnAMB, ZnCMB and ZnPMB was established by decrease in $\log_{10}$ CFU/ml of the test culture after incubation of the plates for 24 h and colony counting. Positive controls were prepared in the same manner, except without adding the samples.

2.6. Statistical analysis

Statistical analysis was done using Student's t-test and one-way ANOVA plus Tukey's test. The results are presented as mean ± standard deviations (SD). Each experimental point was performed in triplicate. The values were considered to be statistically different at $p \leq 0.05$.

3. Results and discussion

3.1. Non-mineralized and Zn-mineralized composite microbeads

Electrostatic extrusion was used to synthesize both non-mineralized (ZnAMB) and Zn-mineralized (ZnCMB and ZnPMB) microbeads. By adding mineral precursors (Na_2HPO_4 or Na_2CO_3) to alginate solution, and subsequent exposure to cross-linking solution, two-phase nanocomposites were made. Zn(II) from the gelling solution mediated simultaneously cross-linking (hydrogel formation) and mineralization process which led to the formation of alginate hydrogel impregnated with a zinc mineral phase. Uniform microbeads, in terms of size and shape, were successfully produced using alginate solution without mineral precursors (ZnAMB) and alginate solution with phosphate mineral precursor (ZnPMB), while microbeads mineralized with carbonate (ZnCMB) were larger in size and appeared less compact and swollen (**Table 2, Fig. 1a-c**).

SEM micrographs of the samples showed a distinctive difference in surface morphology between non-mineralized and mineralized microbeads. Non-mineralized microbeads were smooth (**Fig.**

1d), while mineral precipitates were clearly visible on mineralized microbeads surface (**Fig. 1e** and **1f**). Also, dry mineralized microbeads appeared deformed which can be explained by drying in air and apparently high mineral precursors to Zn(II) from the gelling solution ratio (Xie et al., 2010). Mineralization and gelatination are dynamic and simultaneous processes, and in situations when mineral precursor is present in excess, hydrogel formation is inhibited (*i.e.* due to the formation of a dense surface mineral barrier) which results in not so uniform and stable network. Taking into account that this effect was more pronounced in the case of ZnCMB, which were larger in size due to poor cross-linking and retention of structural water, and also lost the highest amount of water during drying, it can be concluded that not only the concentration, but also the type of mineral precursors affects stability of the obtained nanocomposites.

3.2. XRD analysis

In order to investigate whether alginate, as an organic matrix, affects mineralization process, both free minerals (produced in the absence of alginate by precipitation) and mineralized nanocomposites were characterized by XRD analysis. XRD patterns of Zn-alginate, free minerals and nanocomposite samples are presented in **Fig. 2a** and **2b**.

Free carbonate minerals (**Fig. 2a**) were predominantly composed of $Zn_5(CO_3)_2(OH)_6$, with relatively small amount of $ZnCO_3$ and $Zn_4(CO_3)(OH)_6$. However, in ZnCMB, dominant mineral phase was $Zn_5(CO_3)_2(OH)_6$. The Scherrer equation was used to calculate the crystallite size of free minerals and minerals created within the alginate. The calculated crystallite size of free minerals and minerals within alginate were around 22 and 3 nm, respectively.

Both samples based on phosphate mineral phase were crystallized in the form of $Zn_3(PO_4)_2(H_2O)_4$, but with different morphological properties of crystallites (**Fig. 2b**). Free phosphate crystals showed extreme anisotropic crystallites growth, which resulted in plate-like form with [010] direction that was perpendicular to the flat sides of the crystallites (**Fig. 1h**). On the other hand, phosphate mineral crystallites formed in the presence of alginate, were isotropic yielding to completely random crystallites orientation (**Fig. 1f**). The calculated crystallite size of free phosphate minerals and minerals formed in alginate were around 43 and 28 nm, respectively.

As it can be seen from the obtained results, the formation of crystallites inside alginate matrix is different compared to free mineral formation. Minerals produced in the presence of alginate were smaller, however this effect was more pronounced for carbonate samples where free carbonate crystallites were almost 7 times bigger than minerals within alginate. Phosphate samples exhibited not so drastic change in size (free minerals were double in size when compared to minerals within alginate), but they featured completely different morphologies.

These findings are in good agreement with literature data. As opposed to mineralization in solution, alginate-mediated mineralization is characterized by the presence 3D-fibrilar, porous polymer network and mineralization is restricted to the microenvironments within hydrogel (Mann, 2001). This network can also be considered as a scaffold whereupon mineral phase is formed. Functional groups on polymer matrix and pore density actively affect mineralization process, by changing local concentrations of mineral precursors or nucleation sites formation (Asenath-Smith et al., 2012). It was observed that the presence of alginate affects formation (in terms of size and polymorphism) of calcium carbonate and calcium phosphate crystals (Olderøy et al., 2011; Xie et al., 2010) and Cu-minerals (Bassett et al., 2015). The structural properties of alginate such as monomers composition may also influence the properties of the synthesized mineral phase. Ma and Feng (2011) showed that the length of G-blocks in alginate influenced the morphology and size of $CaCO_3$ synthesized in the presence of alginate. Different biopolymers like pectin (Butler, Glaser, Weaver, Kirkland & Heppenstall-Butler, 2006), chitosan (Hu, Ran, Chen, Shen & Tong, 2015), collagen (Alves et al., 2010) or silk fibroin (Cheng, Shao & Vollrath, 2008) can also be used as matrices for biomineralization. Taking into account that organic and inorganic phase usually closely interact, making in turn composite biomaterial with distinctive properties (Ma, Cohen, Addadi, & Weiner, 2008), this property of alginate could be applied as a good strategy for controllable formation of composite biomaterials with properties tailored to specific biomedical applications.

3.3. FTIR analysis

The FTIR spectra of the samples are presented in **Fig. 2c** and **2d**. The intensive bands at 1091cm^{-1} (O-C-O) and 1029 cm^{-1} (C-O) that can be observed in ZnAMB, represent characteristic bands related to polysaccharide structure (Singh, Sharma, & Gupta, 2009). Free carbonate mineral phase (ZnC) exhibits band at ~3340 cm^{-1} (OH stretching vibrations), while the bands at 1520 cm^{-}

^{1}, 1383 cm^{-1}, 837 cm^{-1} and 709 cm^{-1} originate from carbonate group (Haq & Azad, 2012). The spectrum of free phosphate phase (ZnP) exhibits strong band at ~3350 cm^{-1} due to OH vibrations and bands from PO_4^{3-} vibrations at 1110 cm^{-1}, 1020 cm^{-1} and 940 cm^{-1} (Jung et al., 2009).

FTIR analysis confirmed the presence of carbonate, phosphate and alginate in the nanocomposites. The spectra of phosphate free mineral phase agreed well with spectra of phosphate nanocomposite (ZnPMB). In the spectra of carbonate nanocomposite (ZnCMB) dominate bands related to alginate gel. This could be explained by relatively lower amount of carbonate mineral phase in the nanocomposite compared to phosphate nanocomposite. The changes in the FTIR spectrum of carbonate nanocomposite (*i.e.* the position of carboxyl group band is shifted to 1643 cm^{-1}) indicate the possible chemical interactions of mineral phase with alginate. Xie et al. (2010) also noticed the shifting of the carboxyl group band in alginate after formation of mineral phases. According to the same authors, these interactions between alginate and mineral phases are most probably caused by bonding of metal cations and carboxyl groups in alginate and could be important factor for control of growth of the mineral phase in the presence of polymer.

3.4. Raman spectroscopy

The Raman spectra of non-mineralized and mineralized samples, along with free mineral phases are presented in **Fig. 2e** and **2f**. The Raman spectrum of non-mineralized microbeads, ZnAMB (**Fig. 2e**), is generally in agreement with results previously reported for alginate (Campos-Vallette et al., 2010). The most prominent alginate bands are at 2940 cm^{-1} from C-H vibrations and bands related to alginate uronate units (600-1500 cm^{-1}).

In the Raman spectrum of free carbonate mineral phase (ZnC), the bands characteristic for $Zn_5(CO_3)_2(OH)_6$ can be seen (Falgayrac, Sobanska, & Brémard, 2014; Hales and Frost, 2007). Also, bands identified in the Raman spectrum of free phosphate mineral phase (ZnP) are similar to bands in the previously published data for $Zn_3(PO_4)_2(H_2O)_4$ (Kouisni, Azzi, Zertoubi, Dalard, & Maximovitch, 2004). These findings provide additional support for the data obtained by XRD analysis and clearly show the presence of main constituents in the carbonate and phosphate free mineral phases.

In the Raman spectra of ZnCMB the bands characteristic for alginate dominate, while the Raman spectra of ZnPMB showed more the bands associated with the phosphate mineral phase. Even the intensity of the strong alginate band at 2940 cm^{-1} is reduced in the case of Zn-alginate microbeads with phosphate mineral phase. This may indicate that Raman spectra of mineralized samples showed that formation of phosphate mineral phases on the microbeads surface, and within the alginate is a more consistent process compared to the formation of the carbonate phase, resulting in general better mineralization of ZnPMB. These findings are also in agreement with the results for samples mineral content (Table 2).

3.5. TG analysis

Thermal stability and average mineral phase content of the samples were investigated using TG analysis. TG analysis curves of free minerals, mineralized nanocomposites and non-mineralized samples are presented in **Fig. 3a** and **3b**. Residual masses are following: free zinc carbonate minerals (˜ 72 %), free zinc phosphate minerals (˜ 83 %), non-mineralized Zn-alginate (˜ 18 %), ZnCMB (˜ 31 %) and ZnPMB (˜ 39 %).

TG analysis of ZnAMB indicated four phases of mass loss, as it was expected from the literature (Said & Hassan, 1993): 1) up to temperatures of 170°C, mass loss of ˜ 9 % due to loss of adsorbed water; 2) from 170 to 200°C, ˜ 16 % weight loss due to dehydratation, 3) from 200 to 400°C, ˜ 33 % weight loss due to alginate degradation, leaving zinc carbonate and 4) around 404 – 560°C, further decomposition of zinc carbonate to ZnO and CO_2, causing another ˜ 24 % weight loss. Free zinc carbonate minerals decomposed in two phases (water desorption and calcination) to ZnO and CO_2, while free zinc phosphate minerals remained stable up to 900°C with minor weight loss which could be attributed to the loss of surface water, crystal water and calcination of residual carbonate incorporated during synthesis (Daniel da Silva, Lopes, Gil, & Correia, 2007).

As for the mineralized nanocomposites, it can be seen from **Fig. 3** that the presence of mineral phase has modified thermal degradation properties of the obtained biomaterials. Both nanocomposites exhibited similar degradation patterns up to a certain point: initial weight loss due to water desorption ($T \leq 180°C$), followed by organic phase degradation to zinc carbonate ($180 \leq T \leq 340°C$) and calcination of zinc carbonate to ZnO and CO_2 ($340 \leq T \leq 550°C$). At this

stage, in ZnCMB, deposited zinc carbonate mineral phase continued to decompose contributing to the overall weight loss, while zinc phosphate phase, within ZnPMB, remained stable.

Thermal degradation profiles were also used to calculate the mineral phase content in the nanocomposites (Xie et al., 2010), starting from the assumption that TG curve of mineralized nanocomposite represents a combination of TG curves of free mineral and Zn-alginate. Calculated mineral phase contents in composite samples are presented in **Table 2**. It can be concluded that mineralization process was more efficient in the case of ZnPMB resulting in higher mineral content within hydrogel. Lower mineral content of ZnCMB goes in favor to the conclusion that ZnCMB were poorly cross-linked, with high amount of internal structural water, and low amount of mineral phase.

3.6. Total Zn(II) content

The total zinc loading (expressed as μmol of Zn(II) per g of wet weight) in the obtained samples was determined by ICP-OES. Results are presented in **Table 2**. The presence of zinc-mineral phase in the composites has significantly increased the total metallic loading. Also, phosphate mineralized samples contained more Zn(II) than carbonate. These results are in accordance with literature data (Bassett et al., 2015), where it was shown that the amount of copper within alginate network can be greatly increased by incorporating copper minerals into alginate hydrogels. So, the total Zn(II) content in biomaterials can be modified by changing formulation (introducing mineral phase) and choosing mineral precursor.

3.7. Release kinetics

Stability and release of Zn(II) from non-mineralized and Zn-mineralized microbeads were investigated in static conditions, at 37^{o}C, using DMEM as a release medium. DMEM contains different biomolecules (amino acids, vitamins *etc.*) that actively interact with biomaterial, modifying in turn its stability and solubility (Graddon & Munday, 1961). Zn(II) release profiles from the microbeads are presented in **Fig. 4.**

The cumulative amounts released over incubation period for ZnAMB, ZnCMB and ZnPMB, were: 53.5 ± 2.0, 62.9 ± 1.3 and 70.9 ± 4.4 μmol/g, respectively. It can be observed from **Fig. 4a** that the presence of mineral phase had a significant effect on Zn(II) release, in terms of quantity

and duration. Mineralized samples released more Zn(II) during incubation, which is expected given the higher total Zn(II) content of mineralized samples. Higher total Zn(II) release for ZnPMB when compared to ZnCMB, could be explained by the higher mineral content and higher total Zn(II) content in general (see **Table 2**). In addition, mineralized samples exhibited lower initial burst release, likely due to the presence of superficial mineral barrier. When it comes to stability, mineralized microbeads remained stable during the whole incubation period, while non-mineralized microbeads lost their integrity after 10 days (amorphous precipitate was noticed in the bottom of test tubes). Zn(II) released in the medium over incubation comprised ~34 ~24 and ~21% of the initial Zn(II) loading in ZnAMB, ZnCMB and ZnPMB, respectively (Fig. 4b). Non-mineralized samples released larger portions of metallic loading, and at higher rate, when compared to mineralized ones. Additionally, the release of ˜ 34 % of Zn(II) was apparently high enough to completely disrupt ZnAMB morphology. Mineralized samples exhibited similar trends in % cumulative Zn(II) release during the whole incubation (Fig. 4b). However, taking into account that initial Zn(II) loadings were different in the two nanocomposites, more Zn(II) was released from ZnPMB.

From these results, it can be concluded that mineral deposits within alginate hydrogel network, acted, not only as small reservoirs of Zn(II) which could be further released into environment, but they also contributed to the overall nanocomposite stability, through renewal of internal cross-linking.

3.8. Antimicrobial activity

Results of the antimicrobial testing are presented in **Fig. 5**.

Treatment of *S. aureus* with ZnAMB and ZnCMB resulted in approximately 1 $\log_{10}$ reduction during the first 4 h (**Fig. 5a** and **5b**), while for ZnPMB the number of viable bacteria remained constant (**Fig. 5c**). After 24 h microbicidal effect was established for all tested samples (**Fig. 5**).

When *E. coli* was treated with ZnAMB, ZnCMB and ZnPMB a gradual decline of viable cells was observed within 4 h and was amounted to more than 1 $\log_{10}$ (**Fig. 5**). After 24 h microbicidal activity was detected for ZnAMB and ZnCMB (**Fig. 5a** and **5b**), while treatment with ZnPMB significant decreased viable cells count (**Fig. 5c**). The obtained results are in agreement with literature data where it has been shown that Gram-positive bacteria are more sensitive to Zn(II) than Gram-negative (Soderberg, Agren, Tengrup, Hallmans, & Banck, 1989) due to differences

in bacterial cell wall structure. Taking into account that *E. coli* was not completely eliminated by ZnPMB treatment, which has the highest Zn(II) loading, this could be explained by possible lower solubility of Zn-phosphate minerals in the presence of *E. coli* metabolites.

C. albicans was strongly inhibited after first hour (**Fig. 5**). Reduction of ~ 2 $\log_{10}$ was noticed after treatment with ZnAMB and ZnCMB (**Fig. 5a** and **5b**). ZnPMB showed significant reduction of yeast cells number comparing to control sample, but lower than the first two samples, 1 $\log_{10}$ (**Fig. 5c**). After 4 h, similar activity and significant reduction was noticed for all tested samples, and after 24 h microbicidal effect was established (**Fig. 5**).

According to literature, Zn-based antimicrobial biomaterials are predominantly in the form of composites with ZnO nanoparticles (Bajpai, Jadaun, & Tiwari, 2016; Trandafilovic, Bozanic, Dimitrijevic-Brankovic, Luyt, & Djokovic, 2012), or alginate based systems (Qin, 2008; Straccia et al., 2015). To our knowledge, this is the first example of antimicrobial composite biomaterial which contains Zn within mineral phase. Taking into account prospective bacterial resistance to antibiotics, zinc can be considered an efficient substitute for standard antibiotic therapy.

Conclusion

Zn-mineralized alginate nanocomposites were successfully prepared by electrostatic extrusion. The presence of alginate influenced formation of mineral phase within hydrogel network in terms of crystallite dimensions and polymorphy when compared to free mineral precipitation in solution. Mineral phase in hydrogel interacted with alginate polymer chains which resulted in the formation of nanocomposites with altered chemical and thermal properties. Total Zn(II) content, thermal and *in vitro* stability and potential to release Zn(II) in physiologically relevant environment were significantly affected by the presence and type of Zn-mineral phase. Mineralized samples had higher Zn(II) content and proved to be more stable in biological environment. Also, they released Zn(II) in controllable and sustained fashion when compared to non-mineralized sample. All tested samples exhibited strong antimicrobial effect against *S. aureus* and *C. albicans. E. coli* was completely eliminated after treatment with ZnCMB and ZnAMB, while ZnPMB treatment significantly reduced the number of viable cells after 4 h. The obtained results suggest that alginate-mediated biomineralization, where minerals are salts of essential metallic ions like Zn(II), represents a good strategy for designing bioactive and antimicrobial biomaterials for potential biomedical applications. The synthesis procedure is

simple, cost-effective and has a potential for modifying biomaterial properties by changing production parameters.

Acknowledgements

This work was supported by the Ministry of Education, Science and Technological Development of the Republic of Serbia [Grant III 45019 and Grant OI 172057].

References

Alves, N. M., Leonor, I. B., Azavedo, H. S., Reisab, R. L., & Mano, J. F. (2010) Designing biomaterials based on biomineralization of bone. *Journal of Materials Chemistry, 20,* 2911-1921.

Asenath-Smith, E., Li, H., Keene, E. C., Seh, Z. W., & Estroff, L. A. (2012). Crystal growth of calcium carbonate in hydrogels as a model of biomineralization. *Advanced Functional Materials, 22*, 2891–2914.

Bajpai, S. K., Jadaun, M., & Tiwari, S. (2016). Synthesis, characterization and antimicrobial applications of zinc oxide nanoparticles loaded gum acacia/poly(SA). *Carbohydrate Polymers, 153,* 60-65.

Bassett, D. C., Madzovska, I., Beckwith, K. S., Melo, T. B., Obradovic, B., & Sikorski, P. (2015). Dissolution of copper mineral phases in biological fluids and the controlled release of copper ions from mineralized alginate hydrogels. *Biomedical Materials, 10,* http://doi.org/10.1088/1748-6041/10/1/015006

Bouhadir, K. H., Alsberg, E., & Mooney, D. J. (2001). Hydrogels for combination delivery of antineoplastic agents. *Biomaterials, 22,* 2625–2633.

Busch, S., Schwarz, U., & Kniep, R. (2001). Morphogenesis and structure of human teeth in relation to biomimetically grown fluorapatite-gelatine composites. *Chemistry of Materials, 13,* 3260–3271.

Butler, M. F., Glaser, N., Weaver, A. C., Kirkland, M., & Heppenstall-Butler, M. (2006). Calcium Carbonate crystallization in the presence of biopolymers. *Crystal Growth & Design, 6,* 781-794.

Campos-Vallette, M. M., Chandía, P. N., Clavijo, E., Leal, D., Matsuhiro, B., Osorio-Román, O. I., & Torres, S. (2010). Characterization of sodium alginate and its block fractions by surface enhanced Raman spectroscopy. *Journal of Raman Spectroscopy*, *41*, 758-763.

Cheng, C., Shao, Z., & Vollrath, F. (2008). Silk fibroin regulated crystallization of calcium carbonate, *Advanced Functional Materials, 18,* 2172-2179.

Daniel da Silva, A. L., Lopes, A. B., Gil, A. M., & Correia, R.N. (2007). Synthesis and characterization of porous κ-carrageenan/calcium phosphate nanocomposite scaffolds. *Journal of Materials Science, 42,* 8581-8591.

Donati, I., & Paoletti, S. (2009) Material Properties of Alginates. In B. H. A. Rehm (Ed.), *Alginates: Biology and Applications* (pp. 1-53). Berlin: Springer

Falgayrac, G., Sobanska, S., & Brémard, C. (2014). Raman diagnostic of the reactivity between $ZnSO_4$ and $CaCO_3$ particles in humid air relevant to heterogeneous zinc chemistry in atmosphere. *Atmospheric Environment, 85,* 83-91.

Graddon D. P., & Munday, L. (1961). Some properties of copper(II) *α*-amino-acid chelates: A study of solubilities, visible region and infra-red spectra in relation to crystal structure. *Journal of Inorganic and Nuclear Chemistry, 23,* 231-244.

Green, D. W., Leveque, I., Walsh, D., Howard, D., Yang, X., Partridge, K., Mann, S., & Oreffo, R. O. C. (2005). Biomineralized polysaccharide capsules for encapsulation, organization, and delivery of human cell types and growth factors. *Advanced Functional Materials, 15,* 917-923.

Hales, C. M., & Frost, L. R. (2007). Synthesis and vibrational spectroscopic characterization of synthetic hydrozincite and smithsonite. *Polyhedron, 26,* 4955-4962.

Haq, U. I., & Azad, M. A. (2012). Experimental artifacts for morphological tweaking of chemical sensor materials: Studies on ZnO. *Sensors*, 6, 8259-8277.

Hu, J. X., Ran, J. B., Chen, S., Shen, X. Y., & Tong, H. (2015). Biomineralization-inspired synthesis of chitosan/hydroxyapatite biocomposites based on a novel bilayer rate-controlling model, *Colloids and Surfaces B: Biointerfaces. 136,* 457-464.

Jung, H. S., Oh, E., Shim, D., Park, H. D., Cho, S., Lee, R. B., Jeong, U. Y., Lee, H. K., & Jeong, H. S. (2009). Sonochemical synthesis of amorphous zinc phosphate nanospheres. *Bulletin of the Korean Chemical Society, 10,* 2280-2282.

Kasemets, K., Ivask, A., Dubourguier, H. C., & Kahru, A. (2009). Toxicity of nanoparticles of ZnO, CuO and TiO2 to yeast *Saccharomyces cerevisiae*. *Toxicology in vitro, 6,* 1116-1122.

Kaur, K., Gupta, R., Saraf, S. A., & Saraf, S. K. (2014). Zinc: The metal of life. *Comprehensive Reviews in Food Science and Food Safety*, *13,* 358-376.

Klančnik, A., Piskernik, S., Jeršek, B., & Možina S. (2010). Evaluation of diffusion and dilution methods to determine the antibacterial activity of plant extracts. *Journal of Microbiological Methods, 81,* 124-126.

Kouisni, L., Azzi, M., Zertoubi, M., Dalard, F., & Maximovitch, S. (2004). Phosphate coatings on magnesium alloy AM60 part 1: study of the formation and the growth of zinc phosphate films. *Surface & Coatings Technology*, *185,* 58-67.

Lansdown, A. B. G., Mirastschijski, U., Stubbs, N., Scanlon, E., & Ågren, M. S. (2007). Zinc in wound healing: Theoretical, experimental, and clinical aspects. *Wound Repair & Regeneration, 15,* 2-16.

Lemire, J. A., Harrison, J. J., & Turner, R. J. (2013). Antimicrobial activity of metals: mechanisms, molecular targets and applications. *Nature Reviews Microbiology*, *11,* 371-384.

Ma, Y., Cohen, S. R., Addadi, S., & Weiner, S. (2008). Sea urchin tooth design: An "all-calcite" polycrystalline reinforced fiber composite for grinding rocks. *Advanced Materials, 20*(8), 1555-1559.

Mann, S. (2001). *Biomineralization: Principles and concepts in bioinorganic materials chemistry.* (1st ed.). New York: Oxford University Press

Olderøy, M., Xie, M., Strand, B. L., Draget, K. I., Sikorski, P., & Andreassen, J. P. (2011). Polymorph switching in the calcium carbonate system by well-defined alginate oligomers. *Crystal Growth and Design*, *11,* 520–529.

Qiao, Y., Zhang, W., Tian, P., Meng, F., Zhu, H., Jiang, X., Liu, X., & Chu, P. K. (2014). Stimulation of bone growth following zinc incorporation into biomaterials. Biomaterials, 35, 6882-6897.

Qin, Y. (2008). Alginate fibers: An overview of the production processes and applications in wound management. *Polymer International, 57,* 171-180.

Said, A. A., & Hassan, R. M. (1993) Thermal decomposition of some divalent metal alginate gel compounds. *Polymer Degradation and Stability, 39,* 393-397.

Salih, V., Patel, A., & Knowles, J. C. (2007). Zinc-containing phosphate-based glasses for tissue engineering. *Biomedical Materials, 2,* 11-20.

Shi, J., Zhang, Z., Qi, W., & Cao, S. (2012). Hydrophobically modified biomineralized polysaccharide alginate membrane for sustained smart drug delivery. *International Journal of Biological Macromolecules, 50,* 747-753.

Singh, B., Sharma, D. K., & Gupta, A. (2009). A study towards release dynamics of thiram fungicide from starch-alginate beads to control environmental and health hazards. *Journal of Hazardous Materials, 1,* 208-216.

Soderberg, T., Agren, M., Tengrup, I., Hallmans, G., & Banck, G. (1989). The effects of an occlusive zinc medicated dressing on the bacterial flora in excised wounds in the rat. *Infection, 17,* 81-85.

Straccia, M. C., D'Ayala, G. G., Romano, I., & Laurienzo, P. (2015). Novel zinc alginate hydrogels prepared by internal setting method with intrinsic antibacterial activity. *Carbohydrate Polymers, 125,* 103-112.

Trandafilovic, L. V., Bozanic, D. K., Dimitrijevic-Brankovic, S, Luyt, A. S., & Djokovic, V. (2012). Fabrication and antibacterial properties of ZnO–alginate nanocomposites, *Carbohydrate Polymers, 88,* 263-269.

Tuan, R. S., Boland, G., & Tuli, R. (2003). Adult mesenchymal stem cells and cell-based tissue engineering. *Arthritis Research & Therapy, 5,* 32-45.

Willis, M. S., Monaghan, S. A., Miller, M. L., McKenna, R. W., Perkins, W. D., Levinson, B. S., Bhushan, V., & Kroft, S. H. (2005). Zinc-induced copper deficiency: a report of three cases initially recognized on bone marrow examination. *American Journal of Clinical Pathology, 123,* 125-131.

Xie, M., Olderøy, M., Andreassen, J. P., Selbach, S. M., Strand, B. L., & Sikorski, P. (2010). Alginate-controlled formation of nanoscale calcium carbonate and hydroxyapatite mineral phase within hydrogel networks. *Acta Biomaterialia, 6,* 3665–3675.

Yamaguchi, M. (1998). Role of zinc in bone formation and bone resorption. *Journal of Trace Elements in Medicine and Biology, 11,* 119-135.

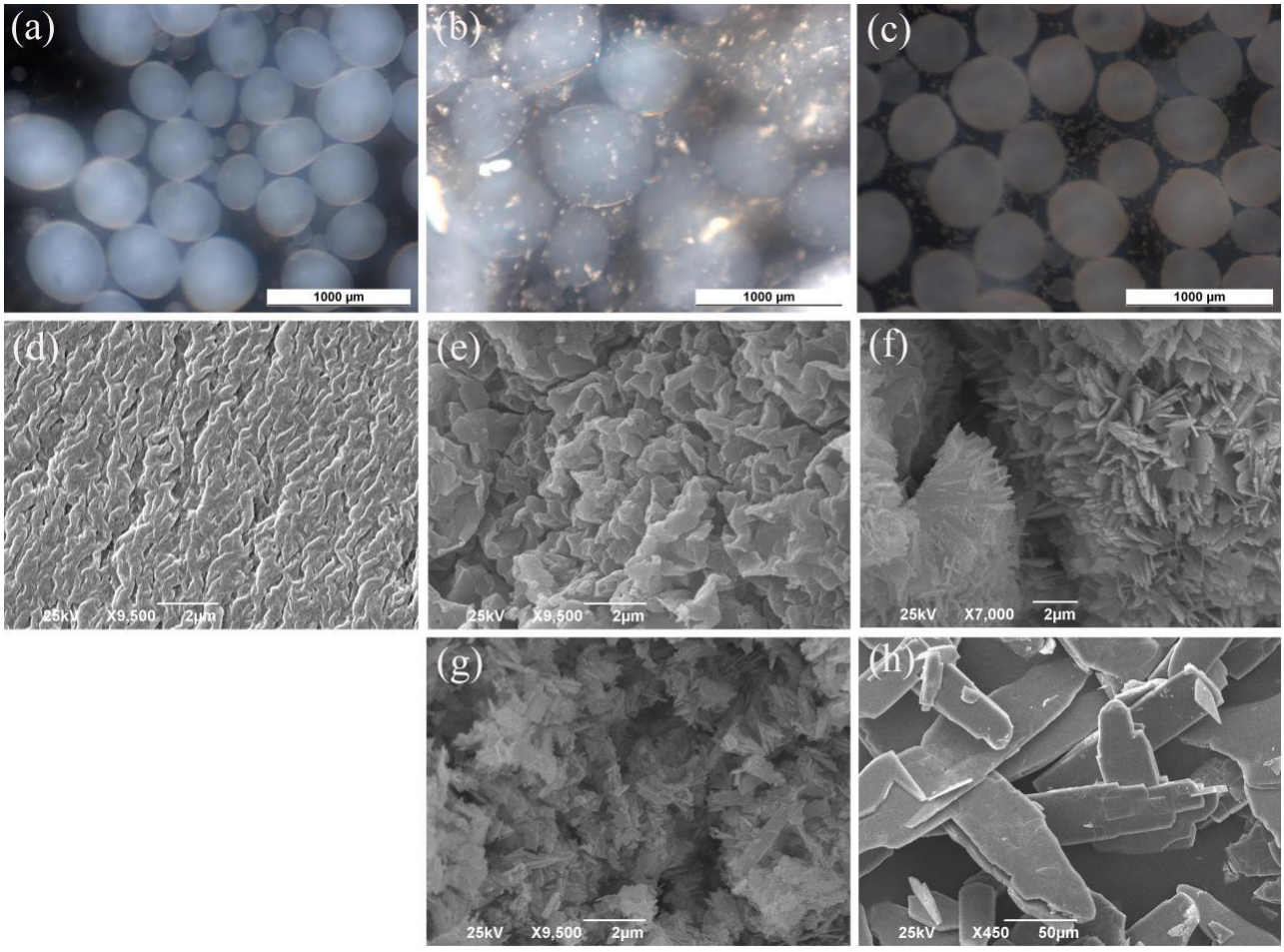

Figure 1. Overall morphology of non-mineralized and Zn-mineralized microbeads: Optical micrographs of: (a) ZnAMB; (b) ZnCMB; and (c) ZnPMB. SEM micrographs of surface: (d) ZnAMB; (e) ZnCMB; (f) ZnPMB. Free minerals: (g) ZnC; and (h) ZnP.

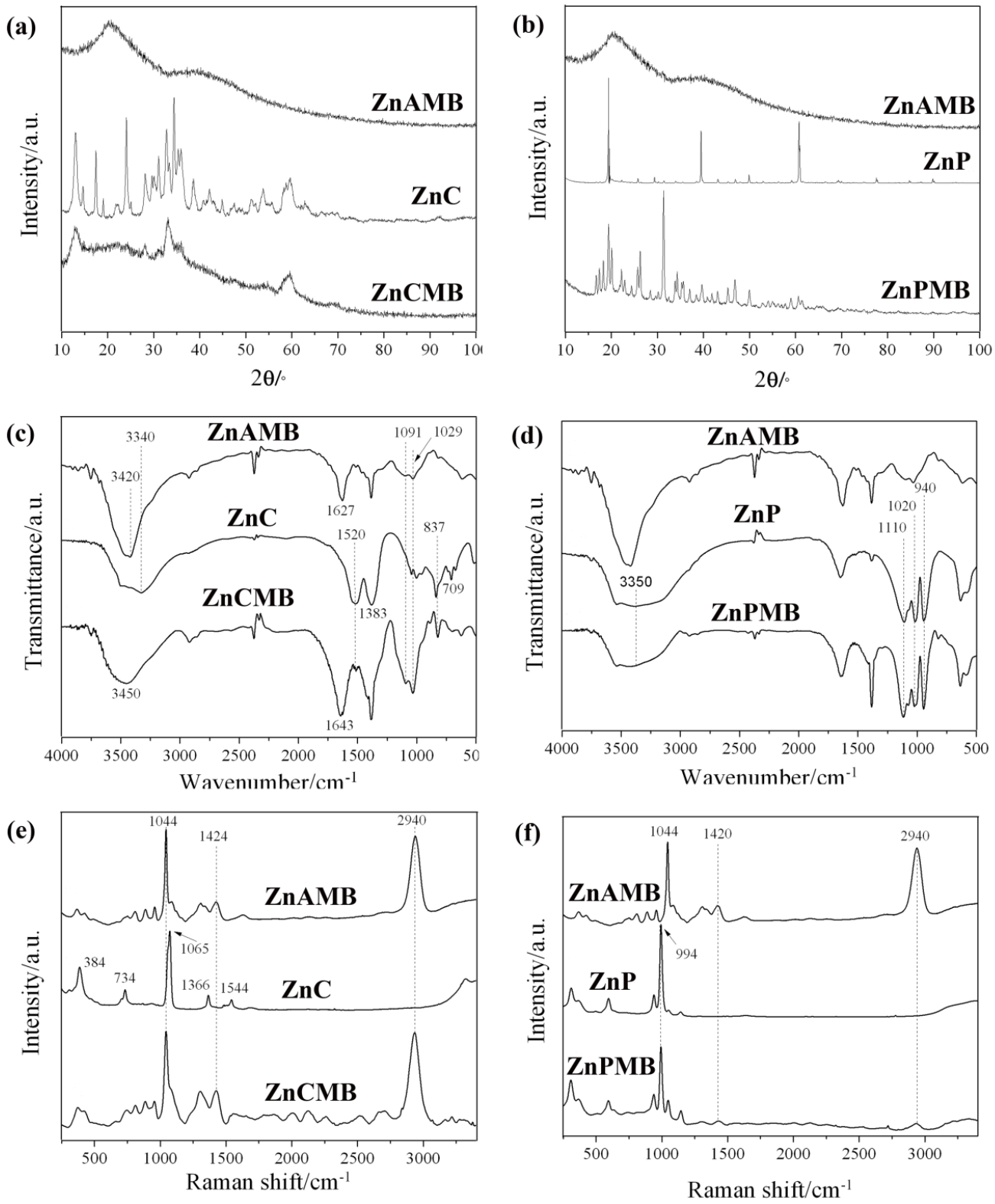

Figure 2. Sample characterization: XRD patterns of: (a) ZnCMB and (b) ZnPMB; FTIR spectra of (c) ZnCMB and (d) ZnPMB; Raman spectra of (e) ZnCMB and (f) ZnPMB.

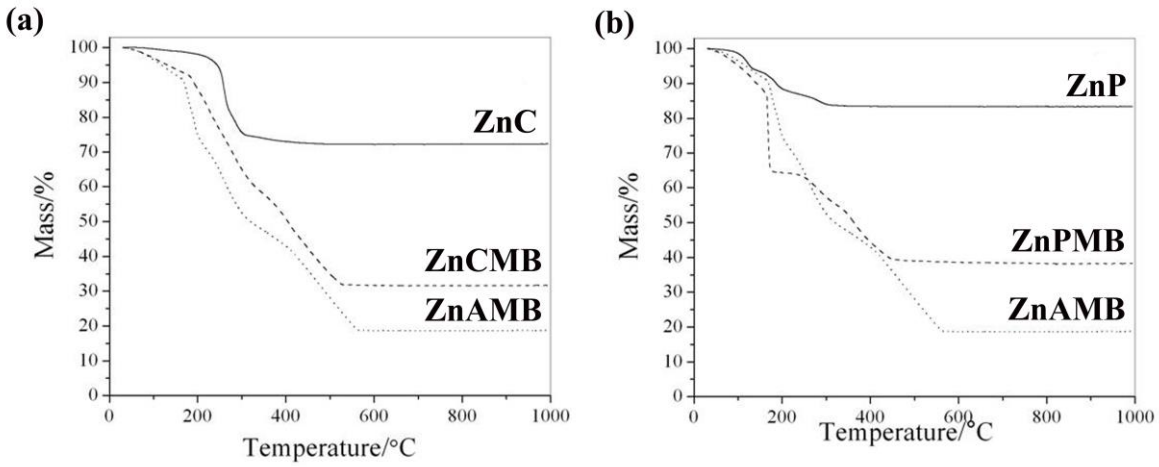

Figure 3. TG analysis for mineralized samples, compared to non-mineralized (ZnAMB) and free mineral samples: a) ZnCMB and b) ZnPMB.

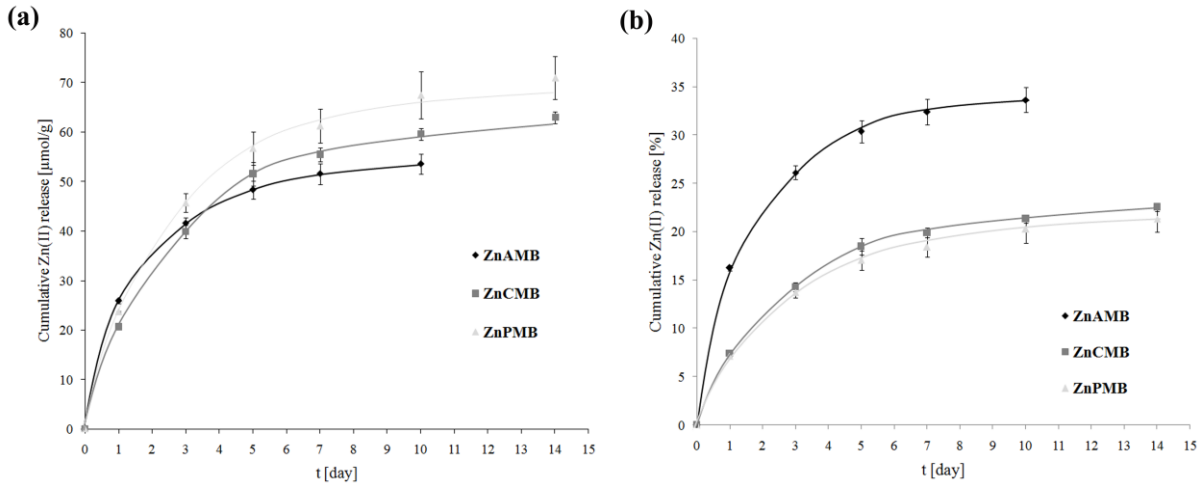

Figure 4. Release profiles of Zn(II) from non-mineralized and Zn-mineralized microbeads in DMEM solution at 37 °C: a) cumulative Zn(II) release over incubation, presented as µmol of Zn(II) per gram of wet microbeads; b) cumulative Zn(II) release presented as the percentage of the initial metallic loading in microbeads.

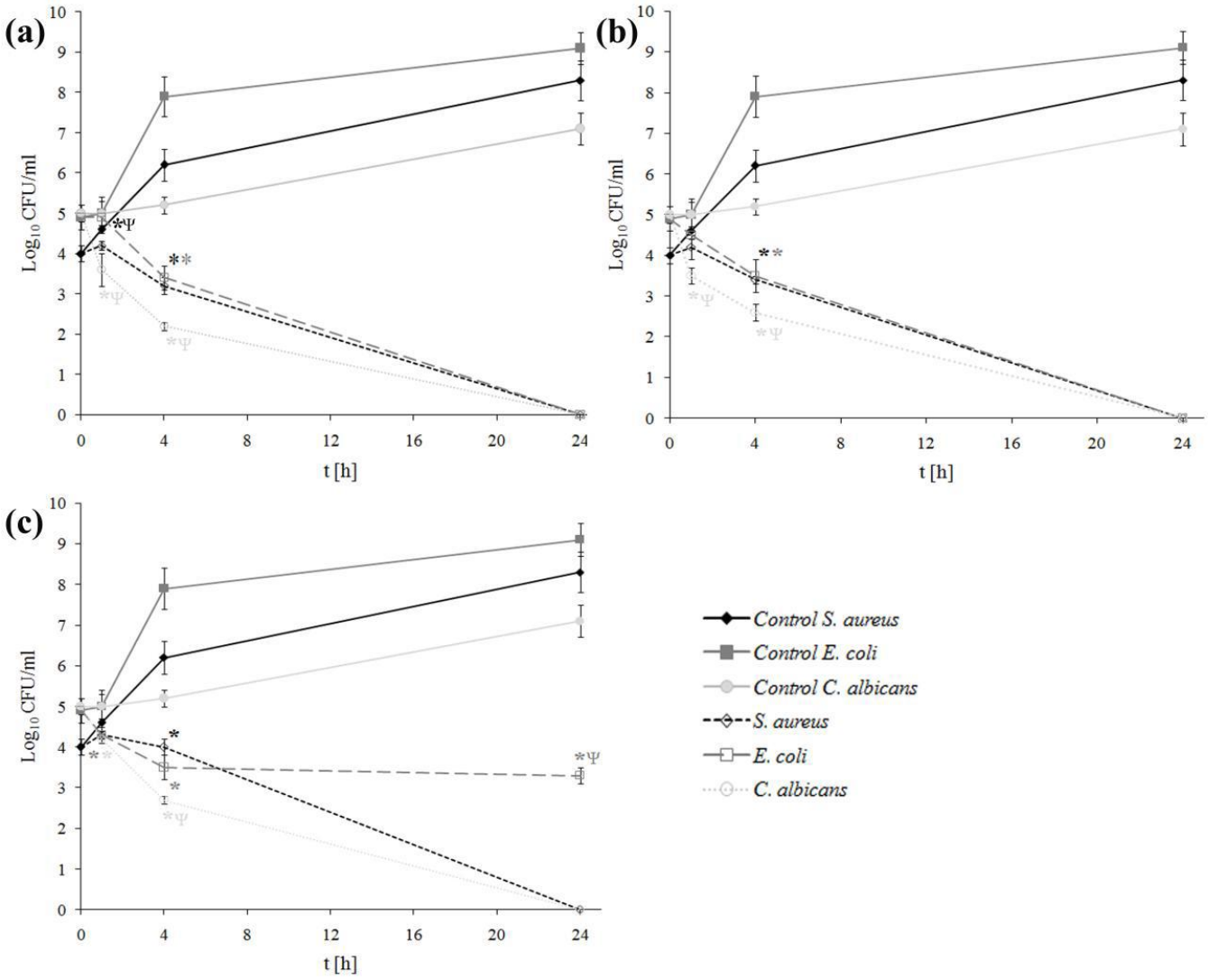

Figure 5. Antibacterial activity of non-mineralized and Zn-mineralized alginate samples against *S. aureus*, *E. coli* and *C. albicans*, expressed as $\log_{10}$ CFU/ml (a) ZnAMB; (b) ZnCMB and (c) ZnPMB. Significant differences compared to control samples are indicated by asterisk ($*p \leqslant 0.05$), significant differences among tested microorganisms within the same time point are indicated by psi, ψ ($\psi p \leqslant 0.05$).

Table 1. Sample abbreviations and formulations.

Sample abbreviation	Extrusion solution		Gelling solution
	Na-alginate	Mineral precursor	
ZnAMB[a]	1.9 % w/v Na-alginate	/	100 mM $Zn(NO_3)_2$
ZnCMB[b]		100 mM Na_2CO_3	
ZnPMB[c]		100 mM Na_2HPO_4	
ZnC[d]	/	Na_2CO_3	
ZnP[e]	/	Na_2HPO_4	

[a] non-mineralized Zn-Alginate MicroBeads
[b] mineralized Zn-Carbonate/Zn-Alginate nanocomposite MicroBeads
[c] mineralized Zn-Phosphate/Zn-Alginate nanocomposite MicroBeads
[d] free Zinc-Carbonate mineral precipitates
[e] free Zinc-Phosphate mineral precipitates

Table 2. Summary of sample groups characteristics and release potential.

Sample	Average size [µm]	Dry weight[a] [%]	Zn(II) content [µmol/g]	Mineral phase content[b] [%]
ZnAMB	461 ± 27	4.5	159 ± 7	/
ZnCMB	670 ± 41	2.9	279 ± 21	24.08
ZnPMB	461 ± 32	7.1	333 ± 17	30.24

[a] Shown as percentage of the initial wet weight
[b] Shown as percentage of dry weight